ASTRONOMY & ASTROPHYSICS
SUPPLEMENT SERIES

*Astron. Astrophys. Suppl. Ser.* **137**, 203–216 (1999)



# 3D mapping of optical turbulence using an atmospheric numerical model

## II. First results at Cerro Paranal

**E. Masciadri**[1], **J. Vernin**[1], **and P. Bougeault**[2]

[1] U.M.R. 6525 Astrophysique, Université de Nice-Sophia Antipolis, Centre National de la Recherche Scientifique, Parc Valrose, 06108 Nice Cedex 2, France
[2] Centre National de Recherches Météorologiques Météo France, 42 Av. G. Coriolis, 31057 Toulouse, France

Received July 17, 1998; accepted February 4, 1999

**Abstract.** The first statistical results of simulations of optical turbulence over Cerro Paranal by an atmospheric non-hydrostatic model (Meso-Nh) are presented. Measurements from the whole PARSCA93 campaign are analyzed. Simulations are compared to optical measurements obtained by a Scidar and a DIMM working at the same time during 14 nights 13-26 May 1993 over Paranal (Chile). An orographic model with a horizontal resolution of 500 m is implemented in Meso-Nh to study its sensitivity to the orographic effects. The model is initialized with radiosoundings profiles provided by Antofagasta station (70.43 W, 23.43 S) and ECMWF analyses extracted from the nearest grid point (70.31 W, 23.62 S) to this meteorological station. A detailed quality study of radiosounding and analyses is presented. No radiosoundings were provided by Antofagasta station during 4 nights and numerical instabilies were generated by the model during the 13 and 26 May 1993 nights. So, only 8 nights were actually studied. Two statistical methods are presented: Method A has a high temporal resolution, Method B has a high vertical spatial resolution. Method A compares integrated values (seeing) provided by simulations and measurements, Method B compares the $C_N^2$ profiles. Different statistical estimators are computed for both the methods. We demonstrate that the model can reproduce well the spatial distribution of the optical turbulence in both the high and low atmospheric regions but the unreliability of Antofagasta radiosoundings hampers the statistical results of the numerical technique. To better test the performance of the model, a comparison between the numerical and the forecasting-by-persistence techniques is presented. With a poor statistical sample (only 8 nights), no conclusive statements can be made about the performances of the two techniques. The model ability to discriminate between the best ($\varepsilon = 0.38$) and the worst ($\varepsilon = 1.38$) nights of the campaign is promising for the future implementation of the numerical technique for flexible scheduling of telescopes.

**Key words:** atmospheric effects — site testing — turbulence

*Send offprint requests to*: E. Masciadri

### 1. Introduction

In the previous paper (Masciadri et al. 1998 - Paper I) we presented the general characteristics of an atmospheric numerical model (Meso-Nh) conceived to provide not only 3D maps of the classic meteorological parameters $P$, $T$, and $\boldsymbol{V}$ but also the $C_N^2$ optical turbulence profiles. We described the dynamical turbulence (Sect. 3.2) and the optical turbulence (Sect. 3.3) parametrization realized in the model. We presented a complete description of the astronomical parameters coded in Meso-Nh (Sect. 3.4). Finally, we discussed the applications of this technique to site testing and flexible scheduling for optimization of the observing time of a telescope. The main questions for an efficient application of the numerical technique concern its sensitivity and statistical reliability. The latter depends mainly on the quality of the initial atmospheric parameters supplied to the model to make a simulation. We intend, in the present paper, to analyze the statistical reliability of the Meso-Nh model comparing simulations with measurements obtained during a 14-night site testing campaign PARSCA93 (Fuchs & Vernin 1994) that took place at Paranal mountain (Chile) in May 1993, in which optical measurements of the seeing were made. The model initialization data used for this study are both radiosoundings provided by Antofagasta station

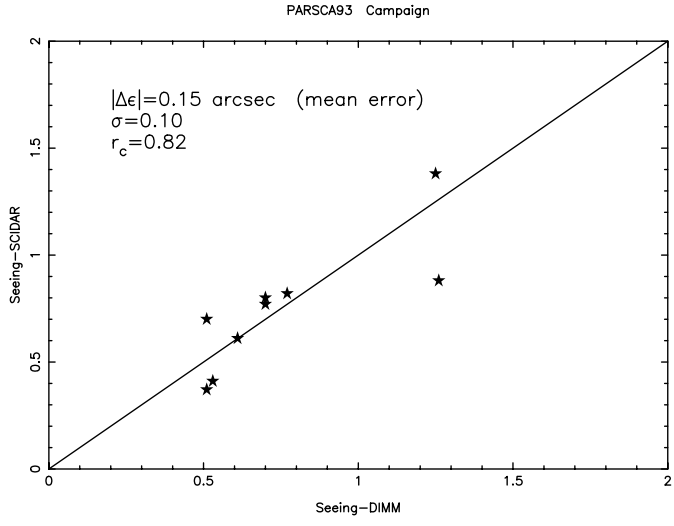


**Fig. 1.** PARSCA93 campaign - Scidar and DIMM seeing measurements. Statistical analysis. $\sigma$ = standard deviation, $r_c$ = correlation coefficient

and ECMWF (European Center for Medium Weather Forecast) analysis computed at an appropriate grid point.

## 2. PARSCA93 campaign

The measurements that are analyzed to test the model simulations are the seeing provided by a DIMM-ESO and the $C_N^2$ profiles provided by a Classic Scidar adapted to a telescope with diameter $D = 84$ cm (Département d'Astrophysique-Nice). From the whole PARSCA93 campaign 13-26 May only 8 nights among 14 have been selected. During the nights of 20, 21, 22 and 24 the Antofagasta station did not provide any radiosounding. The nights of 13 and 26 May have been discarded because they gave rise to numerical instabilities. The nights finally selected were those of the 14, 15, 16, 17, 18, 19, 23 and 25 May 1993.

In Table 1, averaged values of the Scidar and DIMM observations are shown for each night of the campaign. During the whole campaign, the DIMM-ESO ran during a shorter time than the Scidar. In order to compare measurements provided by the two instruments, we averaged the Scidar and DIMM measurements (third and fourth column) on the same time range (fifth column). As can be seen, comparing the third and fourth column, there is a good correlation for most of the cases, the mean absolute difference is $\langle \Delta\varepsilon \rangle = 0.15$ with a standard deviation of $\sigma = 0.10$. The correlation between the Scidar and DIMM measurements ($r_c = 0.82$) is shown in Fig. 1. This statistical analysis has to be kept in mind when the model simulations are compared with optical measurements in Sect. 5. During the PARSCA93 campaign the Scidar was installed about 300 m below the Paranal peak while the DIMM-ESO is at the Paranal level. The two instruments pointed at the same stars during the measurements. Knowing that the Scidar is not sensitive to the scintillation in the low atmosphere, this particular disposition of the instruments is necessary for a good correlation between Scidar and DIMM measurements.

## 3. Initialization data

Two different sort of initialization data have been used: radiosoundings and analyses. In order to make atmospheric forecasts at synoptic scales, a customer has a finite number of observation data available, moreover not uniformly distributed. There are regions, such as ocean, where the observation density is extremely low. Operational meteorological centers can provide the analyses as a result of a sophisticated interpolation of the observations (Annexe 1) to fill the missing information. Then the initial information (observations) becomes spatially uniform but it remains discrete in time.

### *3.1. ECMWF analysis and Antofagasta radiosoundings*

We used for this study the Antofagasta station (70.43 W, 23.43 S) radiosounding profiles and ECMWF analyses computed to the nearest grid point (70.31 W, 23.62 S) to the Antofagasta station provided for all the synoptic hours (00:00 U.T., 06:00 U.T., 12:00 U.T. and 18:00 U.T.). The Antofagasta station provides observations only once a day (12:00 U.T.), instead of twice, as usual in the standard procedure (12:00 U.T. and 00:00 U.T.). This is a problem for the initialization phase of the Meso-Nh model. 12:00 U.T. is about two hours after the end of the night as can be seen in Fig. 2. Throughout the whole campaign, the Scidar observations took place in the first part of the night, between 00:00 U.T. and 05:30 U.T., corresponding to the only double star available. This means that we do not have radiosoundings taken when the Scidar was operated.

The quality of radiosoundings and analysis data is an important aspect of the simulation procedure because initial conditions of low quality may produce erroneous simulation results. To estimate the differences between the radiosoundings and the ECMWF analysis temperature profiles we show the emagrams related to the two cases provided by Meso-Nh. An emagram is a thermodynamical diagram used to describe the atmospheric state. As an example, in Fig. 3 we show, for the 26 May 1993, the radiosoundings emagram at 12:00 U.T. and in Fig. 4 the analysis emagrams at the same hour. The pressure is plotted in ordinates. The isotherms are inclined at 45 degrees and have a linear scale and the adiabats are represented by dashed, bent, transverse lines. The temperature profile is represented by the right side curve. These figures represent just two samples taken from our data, but after a

**Table 1.** PARSCA93 campaign - Seeing measurements from Scidar and ESO-DIMM. In the second column is reported the seeing measured by Scidar. Each value is averaged on the whole night. In the third and fourth column are reported the Scidar and DIMM seeing measuremnts averaged over the same common time range. In the fifth column is reported the time range. In the last column are reported the differences between the measurements from the two instruments. The absolute mean difference is $|\Delta\varepsilon| = 0.15$ and the standard deviation is $\sigma = 0.10$

| Night | $\varepsilon_{SCI}$ $(arcsec)$ | $\varepsilon^*_{SCI}$ $(arcsec)$ | $\varepsilon_{DIMM}$ $(arcsec)$ | Time Range (U.T.) | $\lvert\Delta\varepsilon\rvert$ |
|---|---|---|---|---|---|
| 13/5 | 0.87±0.25 | - | - | - | - |
| 14/5 | 0.99 | - | - | - | - |
| 15/5 | 0.81 | 0.82±0.29 | 0.77±0.29 | 1.15-5.45 | 0.05 |
| 16/5 | 1.38 | 1.38 | 1.25 | 1.00-5.40 | 0.13 |
| 17/5 | 0.83 | 0.88 | 1.26 | 2.63-4.45 | -0.38 |
| 18/5 | 0.93 | - | - | - | - |
| 19/5 | 0.80 | 0.77 | 0.70 | 2.52-5.15 | 0.07 |
| 20/5 | 0.40 | 0.41 | 0.53 | 2.85-5.28 | -0.12 |
| 21/5 | 0.67 | 0.70 | 0.51 | 0.00-4.95 | 0.19 |
| 22/5 | 0.67 | 0.80 | 0.70 | 3.05-5.16 | 0.10 |
| 23/5 | 0.66 | - | - | - | - |
| 24/5 | 0.63 | 0.61 | 0.61 | 0.68-4.17 | 0.00 |
| 25/5 | 0.38 | 0.37 | 0.51 | 2.40-4.78 | -0.14 |
| 26/5 | 0.57 | - | - | - | - |

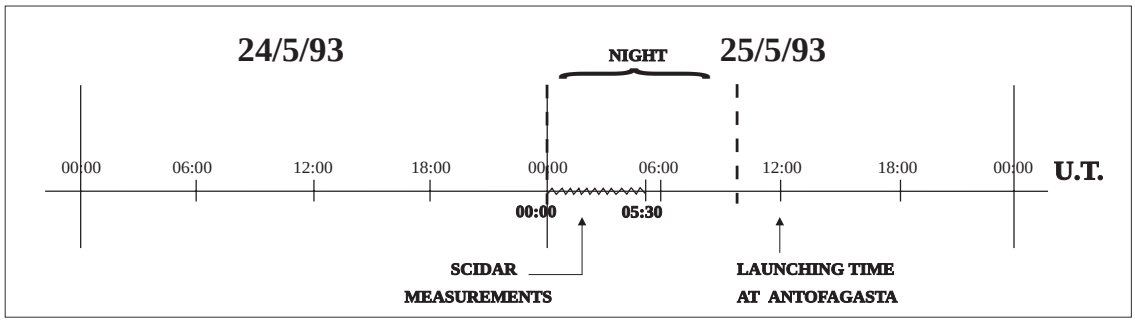


**Fig. 2.** Scidar measurements and radiosoundings data location in a observation temporal scale

complete analysis of all the campaign emagrams, we can make the following general remarks: the radiosoundings temperature profile resolution is higher than that provided by the meteorological analysis. Moreover, the thermal inversion of low layers (below 850 hPa) is not detected in the analysis data whereas it appears in the radiosoundings. The temperature profiles given by radiosoundings in the higher layers do not reproduce the typical thermal inversion above the tropopause (at around 150 hPa). A possible explanation of the low vertical resolution of the analysis data is that they are calculated at only 15 levels, introducing an important averaging effect.

The analysis temperature profiles have a low vertical resolution provided by a spatial (vertical) and temporal interpolation process. The temporal resolution is limited by the fact that observations are taken only once a day. The intensity and wind directions, taken from radiosoundings and analyses at 12:00 U.T. are better correlated. Few discrepancies are found especially at low atmospheric levels.

How do we choose the best initialization criterion? It is not possible to use simple radiosounding or analysis temperature profiles for the reasons just presented. The model must be fed by wind and temperature profiles which best represent the atmospheric behavior at this latitude, in term of thermodynamic equilibrium. For this reason, considering the low resolution of the analysis data, we thought that the best solution was to mix the radiosoundings and the analyses: *we used the radiosounding temperature profile between* 1000 hPa *and* 150 hPa *and the analysis above* 150 hPa. In Fig. 5 we show, as an example, the result of such a mixing between the radiosounding and analysis shown in Fig. 3 and Fig. 4. In this way, we hope to preserve the best vertical resolution. Knowing that the orographic effects are particularly sensitive to the wind near the ground, we used in the low part of the atmosphere (1000 hPa − 750 hPa), the analysis wind direction and

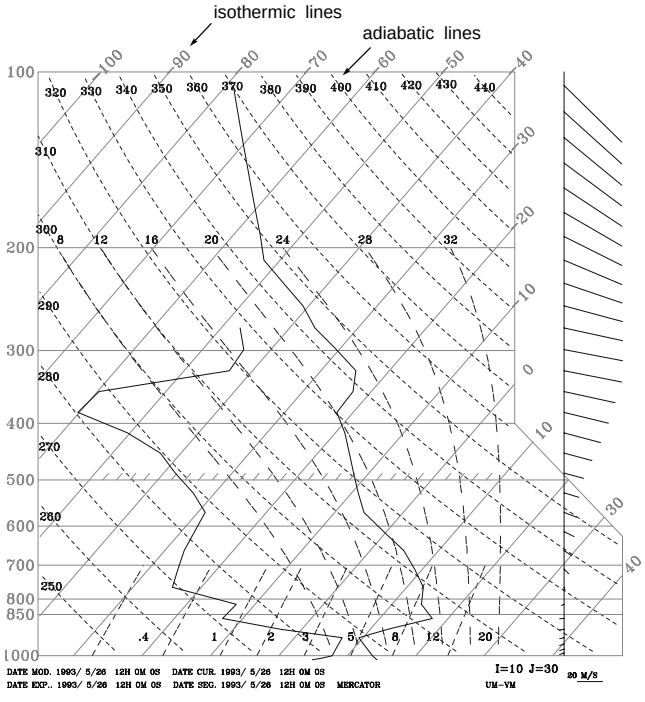


**Fig. 3.** Radiosounding emagram - 26 May 1993 at 12:00 U.T. An emagram is a characteristic thermodynamic diagram used by meteorological stations for the graphic description of the atmosphere state. Units: left scale in hPa, right scale in K degres. The isothermic lines are inclined to 45 degrees and have a linear scale. The adiabatic lines are represented by dashed, bent, transverses lines. The left line represent the dew point temperature and the right line the absolute temperature. The regions in which the absolute temperature line is parallel to the adiabatic lines corresponds to dynamic instability regions. On the right side of figure is reported the wind direction and intensity along on the West-East direction. No warming is visible in the stratosphere (above 150 hPa)

intensity at 00:00 U.T., that is the nearest temporal wind data in this region of the atmosphere.

### *3.2. Initialization data reliability*

After analyzing the whole campaign, an unrealistic radiosounding temperature profile caused the generation of numerical instabilities on two occasions and simulations could not be terminated. We show here an example of the outputs provided by the model in which a numerical instability is detected. Figure 6 shows the seeing time evolution over the Paranal mountain for the 13 May 1993 night. After 200 s, the model generates a dynamic instability caused by the presence of a quasi-null gradient of potential temperature ($\frac{\partial\theta}{\partial z} \sim 0$) at about 10.5 km with a 2 km depth as seen in Fig. 7 (absolute temperature parallel to the adiabats). The presence of a strong wind gradient, coupled with a low potential temperature gradient induces

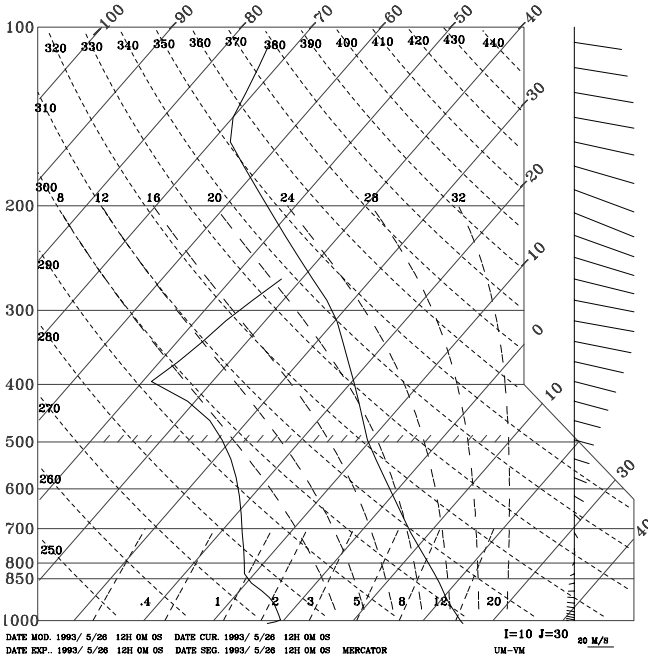


**Fig. 4.** Analysis emagram - 26 May 1993 at 12:00 U.T. - Same as Fig. 3. The stratospheric warming is noticed. The thermic inversion at ground levels (under 750 hPa) is lost

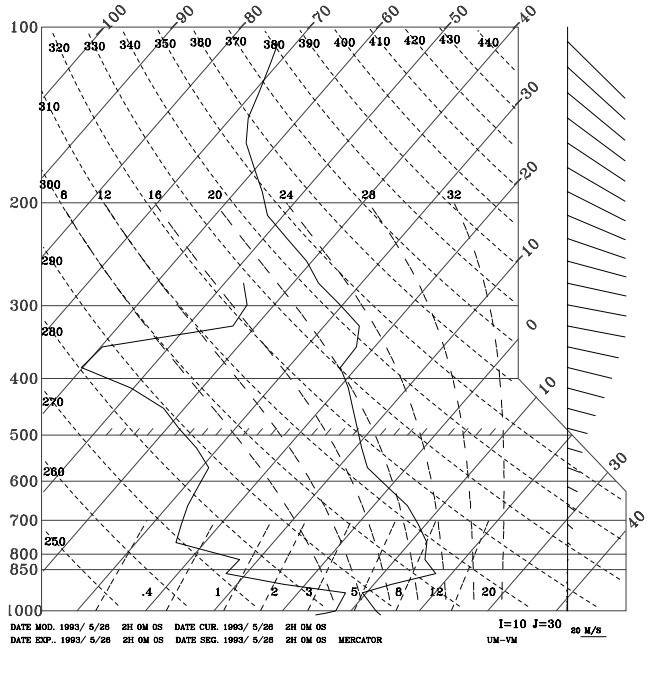


**Fig. 5.** Initialization Emagram - 26 May 1993 (same presentation as Fig. 3). The radiosounding temperature profile (1000 hPa − 150 hPa) is corrected at high levels (over 150 hPa) by the analysis data. In the low atmosphere levels (1000 hPa − 750 hPa) the analysis wind direction and amplitude are used

a Richardson number $R_i < 0.25$ at this altitude, as seen in Fig. 8. Figure 9 shows the $C_N^2$ profile generated by the model along with the profile measured by Scidar on the same night. Evidently, a wrong radiosounding can trigger numerical instability.

## 4. Scidar/Meso-nh statistical comparison

### *4.1. Model configuration*

The spatio-temporal model configuration is the same as described in Paper I. The orographic model, centered above Paranal (70.40 W, 24.61 S), has a 500 m horizontal resolution over a total surface of 60 km × 20 km, that is 120 × 40 grid points (Fig. 1 in Masciadri et al. 1998). A physical time step $t_s = 2.5$ s was used and the following vertical resolution was chosen: an increasing vertical step from 50 m to 245 m between ground level to 3 km and a constant resolution of 600 m up to 20 km.

### *4.2. Statistical analysis*

To test the capacity of the Meso-Nh model to predict seeing, we used Scidar as the reference. Scidar has been tested in many ways, in various sites and compared with other techniques such as DIMM and balloons. Moreover, in Sect. 2 we proved that during the PARSCA93 campaign the correlation between Scidar and DIMM-ESO was good. We compared Scidar and Meso-Nh seeing values during each selected night and we analyzed the correlation between the measurements and simulations. During the worst seeing night we noticed that the seeing increased suddenly after about 3 hours due to the occurrence of a $C_N^2$ layer at 4 km, also seen by the Scidar. Thus, we decided to make 4 hours simulations for each night and we analyzed all the forecasts ranging between 30 min and 4 hours. The first 30 min are discarded because we verified that, for all the simulations, the flow is not yet adapted to the orography. Being aware that our statistical sample is poor (8 nights only) we tried to extract the most complete information with the available data using different techniques. We used two methods that will be named Method A and Method B. For both methods we calculated a linear regression fit and computed the following statistical estimators:

- The correlation coefficient.
$$r = \frac{\sum_i x_i y_i}{\sqrt{\sum_i x_i^2 \sum_i y_i^2}}. \quad (1)$$
where $x_i$ and $y_i$ are the seeing estimated with Scidar and Meso-Nh.
- The correlation coefficient for centered variables
$$r_c = \frac{\sum_i (x_i - \overline{x})(y_i - \overline{y})}{\sqrt{\sum_i (x_i - \overline{x})^2 \sum_i (y_i - \overline{y})^2}}. \quad (2)$$
This gives a more significant estimation of correlation because it is independent of the mean values which are always positive, like seeing.
- The estimator $P$ of the correlation coefficient.
To estimate the reliability of the correlation coefficient we computed the probability $P$ that two uncorrelated distributions of the analyzed data give a correlation coefficient greater than that observed.
- The standard deviation $\sigma$ between Scidar measurements and the regression straight line is
$$\sigma^2 = \frac{1}{N-1} \sum_i (y_i - a x_i)^2 . \quad (3)$$

#### 4.2.1. Method A: High temporal resolution

In this method we compare the seeing deduced from Scidar measurements with the Meso-Nh simulations above Paranal every 2.5 s. In order to have a better estimation of the correct adaptation time, we considered the seeing averaged over different time intervals and we computed the statistical parameters defined before for each interval. In Table 2 we report the statistical results obtained over 6 different time intervals over a complete $4^h$ simulation time: $[1^h - 2^h]$, $[2^h - 3^h]$, $[3^h - 4^h]$, $[1^h - 3^h]$, $[2^h - 4^h]$ and finally $[1^h - 4^h]$. This method gives good temporal statistics but does not give any information about the vertical structure of the optical turbulence.

#### 4.2.2. Method B: High spatial vertical resolution

As we are interested not only in the seeing prediction but also in the turbulent profile prediction, for each night we compared the $C_N^2$ averaged profiles from the Scidar with those obtained from the Meso-Nh output every 30 min. So doing, we have direct access to the temporal evolution of $C_N^2$ profile, that is the optical turbulence evolution at all the model levels.

For each night, we splitted the atmosphere into two regions: we computed the contribution of the boundary layer (BL) defined here between ground level and 5 km and that of the free atmosphere (FA) above 5 km. The same splitting has been used for both Scidar and Meso-Nh. As we are not completely confident in the ability of the Scidar to measure the optical turbulence in the surface layer (first hundred of meters) nor in the Meso-Nh model, we used two sets of Meso-Nh outputs, with and without the surface layer in order to evaluate the sensitivity of the numerical model to the orographic effect. We thus defined a $\varepsilon_{BL}$, a $\varepsilon_{FA}$ and a $\varepsilon_{TOT}$ in the following way

$$\varepsilon_{BL} = 5.30 \lambda^{-1/5} \left( \int_{h_0}^{5000} C_N^2(h) \mathrm{d}h \right)^{3/5} \quad (4)$$

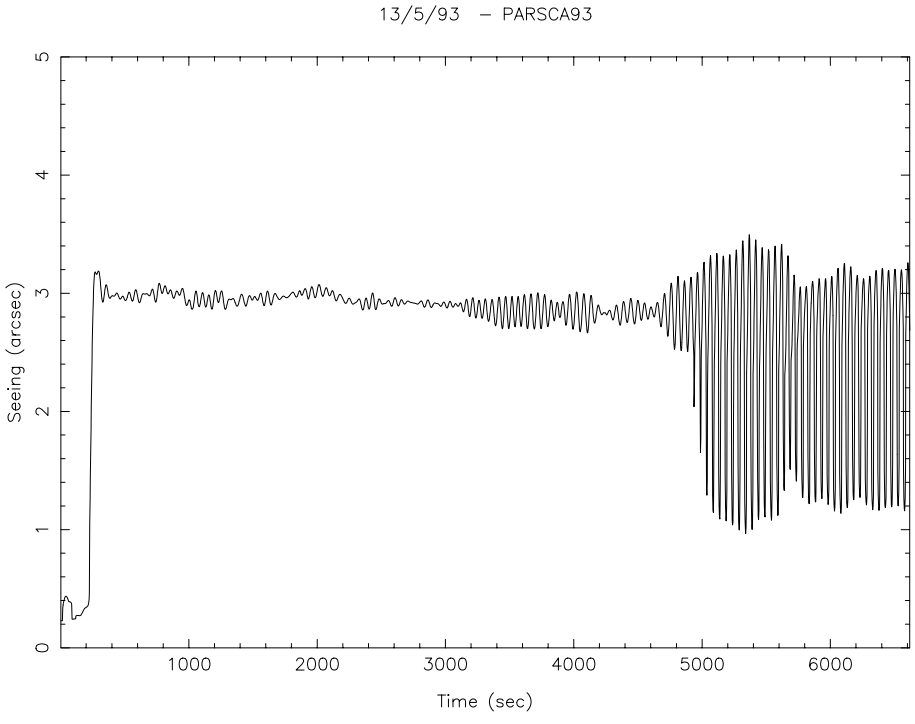


**Fig. 6.** Seeing temporal evolution over 4 hours simulations time above Paranal mountain during the 13 May 1993 night. A numerical instability appears due to unrealistic initial conditions

**Table 2.** Method A: statistical analysis summary. $\alpha$ = calibration coefficient, $a$ = regression line slope, $r$ = correlation coefficient, $r_c$ = centered correlation coefficient, $\sigma$ = standard deviation of the Meso-Nh distribution data with respect to the regression straight line, $P$ = probability that two uncorrelated distribution $x_i$ and $y_i$, belonging to the same parent distributions of the analyzed data, give a correlation coefficient larger than that observed

| | $[1^h - 2^h]$ | $[2^h - 3^h]$ | $[3^h - 4^h]$ | $[1^h - 3^h]$ | $[2^h - 4^h]$ | $[1^h - 4^h]$ |
|---|---|---|---|---|---|---|
| $\alpha$ | 1.57 | 1.43 | 1.52 | 1.47 | 1.47 | 1.52 |
| a | 0.92 | 0.96 | 0.93 | 0.94 | 0.94 | 0.93 |
| $r$ | 0.87 | 0.88 | 0.87 | 0.88 | 0.88 | 0.87 |
| $r_c$ | 0.09 | 0.29 | 0.14 | 0.20 | 0.22 | 0.14 |
| $\sigma$ | 0.51 | 0.48 | 0.50 | 0.48 | 0.48 | 0.50 |
| P($r$) | 0.83 | 0.49 | 0.74 | 0.63 | 0.60 | 0.74 |

$$\varepsilon_{\rm FA} = 5.30\lambda^{-1/5}\left(\int_{5000}^{\infty} C_{\rm N}^2(h){\rm d}h\right)^{3/5} \quad (5)$$

$$\varepsilon_{\rm Tot} = 5.30\lambda^{-1/5}\left(\int_{h_0}^{\infty} C_{\rm N}^2(h){\rm d}h\right)^{3/5} \quad (6)$$

for $\lambda = 0.5\ 10^{-6}$ m.

- **Method B(I)**: $h_0 = 2676$ m, we removed the first 106 m $[3 \leq N \leq 40]$.
- **Method B(II)**: $h_0 = 2560$ m, we kept all the vertical levels $[1 \leq N \leq 40]$.

We underline that the ground level altitude is 2560 m and not 2640 m (the true Paranal altitude) because of an average effect due to the horizontal model resolution used. The second method B is less well statistically defined than the method A. We can average, in fact, only 4 $C_{\rm N}^2$ profiles for each night related to the $1^{\rm h}$, $2^{\rm h}$, $3^{\rm h}$ and $4^{\rm h}$ outputs, but we can analyze the model sensitivity in the first 100 m. In Table 3 and Table 4 are reported the statistical results for two different configurations. We estimated that this test was necessary because we often found that a strong $C_{\rm N}^2$ layer was produced by the model at this low altitude. At the moment we have no a priori reasons to reject or accept this contribution because we know that the Scidar sensitivity at this altitude is poor. Scidar is based on scintillation measurements and it is particularly sensitive to the high troposphere turbulence. The Generalized configuration is sensitive to the low levels turbulence too. During this campaign only a Classic version of Scidar was employed.

**Table 3.** Method B(I): statistical analysis summary. The first 100 m (first two model levels) are rejected. $\beta$ = calibration coefficient. For $a$, $r$, $r_c$, $\sigma$ and $P$, same as Table 2. $\varepsilon_{\rm Tot}{}^*$ is identical to the $[2^{\rm h} - 3^{\rm h}]$ column of Table 2

| $\beta = C_N^2$ correction coefficient= 2.46 - Vertical Levels [3-40] | | | | |
|---|---|---|---|---|
| | $\varepsilon_{Tot}\,(SCI-MNH)$ | $\varepsilon_{BL}\,(SCI-MNH)$ | $\varepsilon_{FA}\,(SCI-MNH)$ | $\varepsilon^*_{Tot}\,(SCI-MNH)$ |
| a | 0.97 | 0.73 | 1.18 | 0.95 |
| $r$ | 0.88 | 0.73 | 0.77 | 0.88 |
| $r_c$ | 0.33 | 0.30 | 0.06 | 0.29 |
| $\sigma$ | 0.54 | 0.55 | 0.42 | 0.48 |
| P($r$) | 0.43 | 0.46 | 0.89 | 0.49 |

**Table 4.** Method B(II): statistical analysis summary. Same as Table 3 but with all the 40 vertical levels

| $\beta = C_N^2$ correction coefficient= 1.88 - Vertical Levels [1-40] | | | | |
|---|---|---|---|---|
| | $\varepsilon_{Tot}\,(SCI-MNH)$ | $\varepsilon_{BL}\,(SCI-MNH)$ | $\varepsilon_{FA}\,(SCI-MNH)$ | $\varepsilon^*_{Tot}\,(SCI-MNH)$ |
| a | 0.94 | 0.83 | 0.91 | 0.95 |
| $r$ | 0.88 | 0.79 | 0.77 | 0.88 |
| $r_c$ | 0.20 | 0.13 | 0.05 | 0.29 |
| $\sigma$ | 0.49 | 0.52 | 0.32 | 0.48 |
| P($r$) | 0.63 | 0.76 | 0.89 | 0.49 |

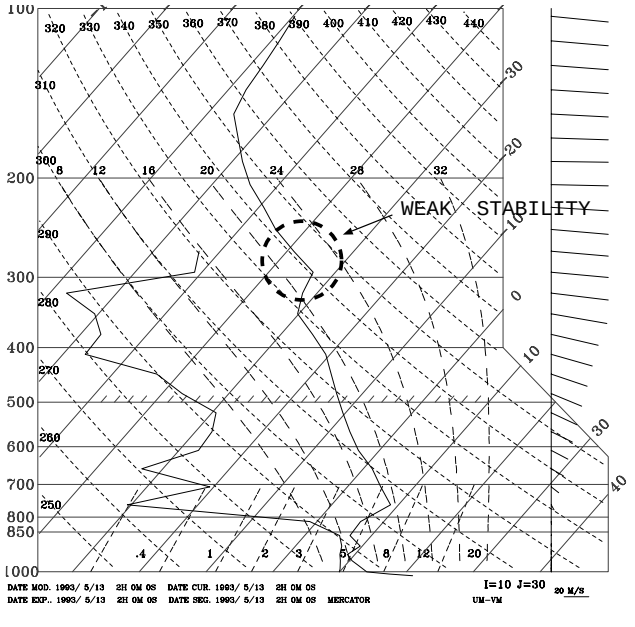


**Fig. 7.** Initialization emegram - 13 May 1993 (same as Fig. 3). A large region of low static stability is present at 300 hPa about

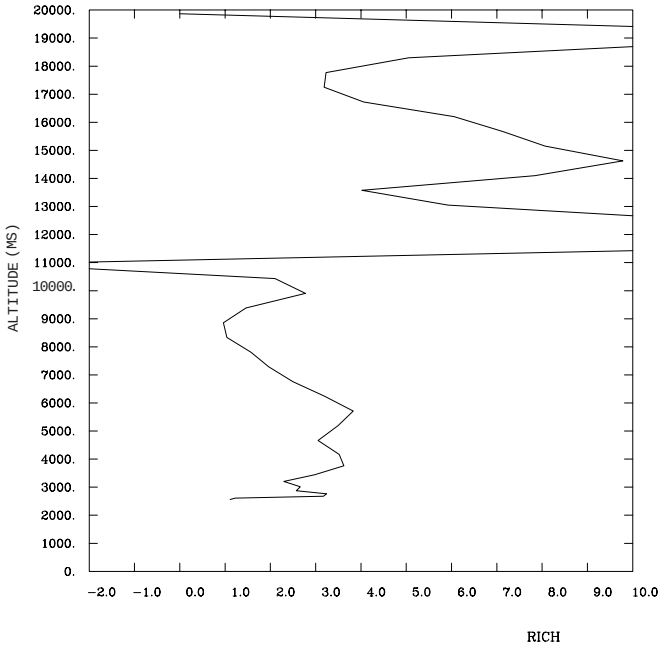


**Fig. 8.** Richardson number profile above Paranal during the 13 May 1993. A dynamic instability is present around 11 km

*4.3. Significance of statistical estimators*

Having a small amount of data, the correlation coefficient $r_{\rm c}$ is a poor estimator for deciding whether an observed correlation is statistically significant or not. $r_{\rm c}$ tells how good is the fit to a straight line but ignores of the individual distributions $x_i$ and $y_i$.

We therefore compute the probability P that two uncorrelated distributions $x_i$ and $y_i$ (belonging to the same parental distribution) give a correlation coefficient greater than that found. A large $P$ means that $r_{\rm c}$ is poor, while a small $P$ means that $r_{\rm c}$ is good. A classic test (Press et al. 1989), adapted for a small amount of data, ($N < 20$) gives the results reported in the Tables 2–4.

The standard deviation of data from the linear regression line might estimate in a complementary way, the data dispersion around the optimized regression line. We report the values in Tables 2-4.

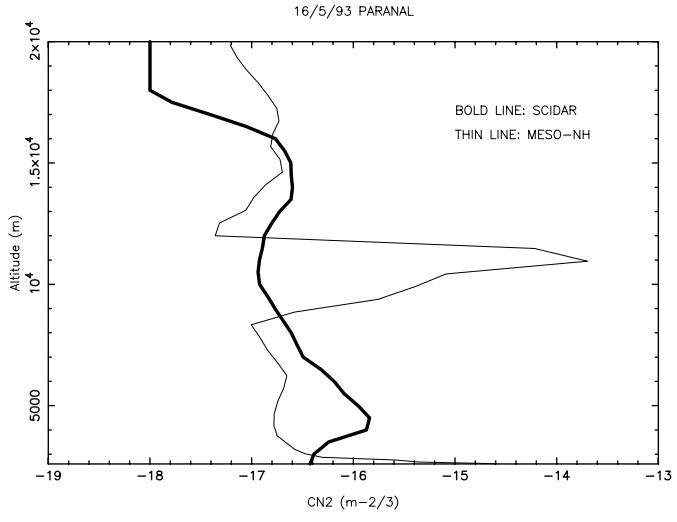


**Fig. 9.** $C_{\rm N}^2$ profiles simulated by the model (thin line) and measured by Scidar (bold line) during the 13 May 1993 night. A large $C_{\rm N}^2$ layer is present at 11 km about

### *4.4. Calibration of simulations*

In both methods A and B we made a calibration of the Meso-Nh outputs using the following procedure. We compute the mean value of Scidar seeing measured $\langle\varepsilon_{\rm SCI}\rangle$ and the Meso-Nh simulated seeing $\langle\varepsilon_{\rm MNH}\rangle$. All the simulated values are multiplied by the calibration coefficient $\alpha = \frac{\langle\varepsilon_{\rm SCI}\rangle}{\langle\varepsilon_{\rm MNH}\rangle}$, before doing any statistical analysis as described in Method A and B. In Method B, the calibration coefficient is named $\beta$.

## 5. Discussion

Using **Method A** (Table 2), we can conclude that the temporal window $[2^{\rm h} - 3^{\rm h}]$ seems to give the best results following the criterion of the greatest correlation coefficient ($r_{\rm c} = 0.29$) . One can observe also that, for this time interval, the probability $P$ that two uncorrelated distributions give a correlation coefficient greater than that found with the actual measurements, is the smallest ($P = 0.49$). In Fig. 10 we show a graphic global analysis of these data.

Using **Methods B(I)-B(II)** (Tables 3-4), we observe that when computed without the first 106 m, a better correlation ($r_{\rm c} = 0.33$) is achieved than with the first 106 m ($r_{\rm c} = 0.20$). The criterium of the minimum standard deviation, leads to the opposite conclusion, i.e. $\sigma$ computed with the first 106 m ($\sigma = 0.50$) is better than that obtained without the surface layer ($\sigma = 0.54$). In Figs. 11-13 we show the data of Table 3 analyzed with the Method B(I) and in Figs. 14-16 the data of Table 4 analyzed with the Method B(II). The Meso-Nh $\varepsilon_{\rm FA}$ values are different in the two Methods B(I) and B(II) because the calibration coefficient is computed using the seeing over the whole atmosphere $\varepsilon_{\rm TOT}$. We emphasize that method B only, based

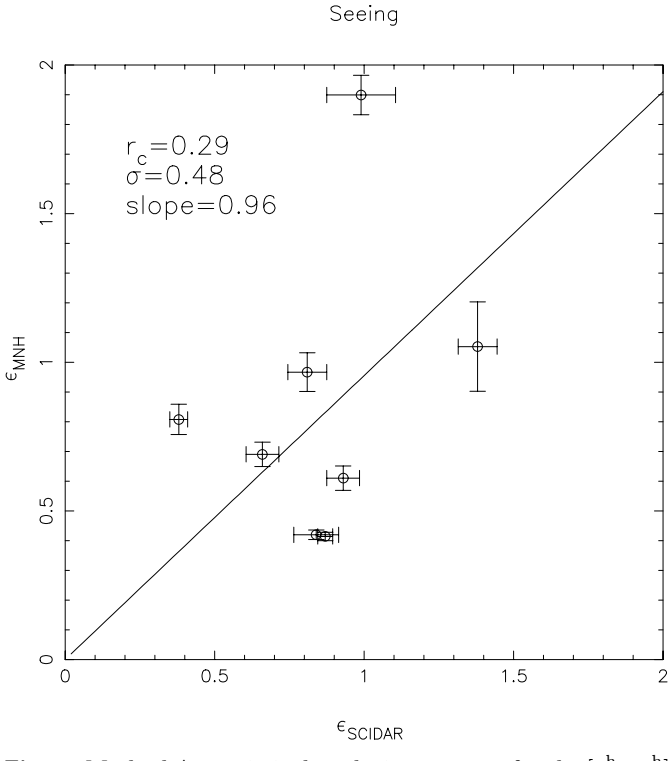


**Fig. 10.** Method A: statistical analysis summary for the $[2^{\rm h} - 3^{\rm h}]$ temporal window. The calibration coefficient is $\alpha = 1.43$ (Table 2)

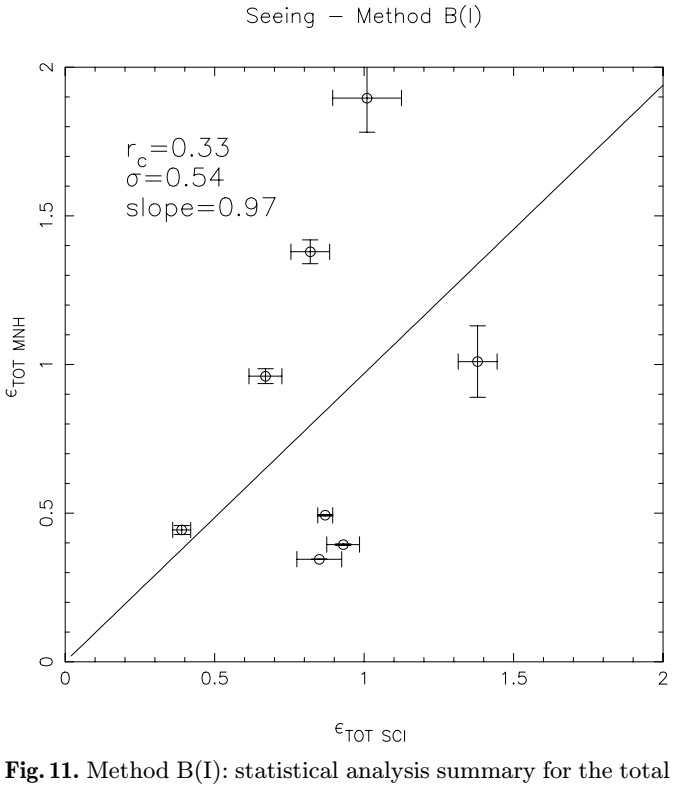


**Fig. 11.** Method B(I): statistical analysis summary for the total seeing $\varepsilon_{\rm Tot}$. The calibration coefficient is $\beta = 4.48$ (Table 3)

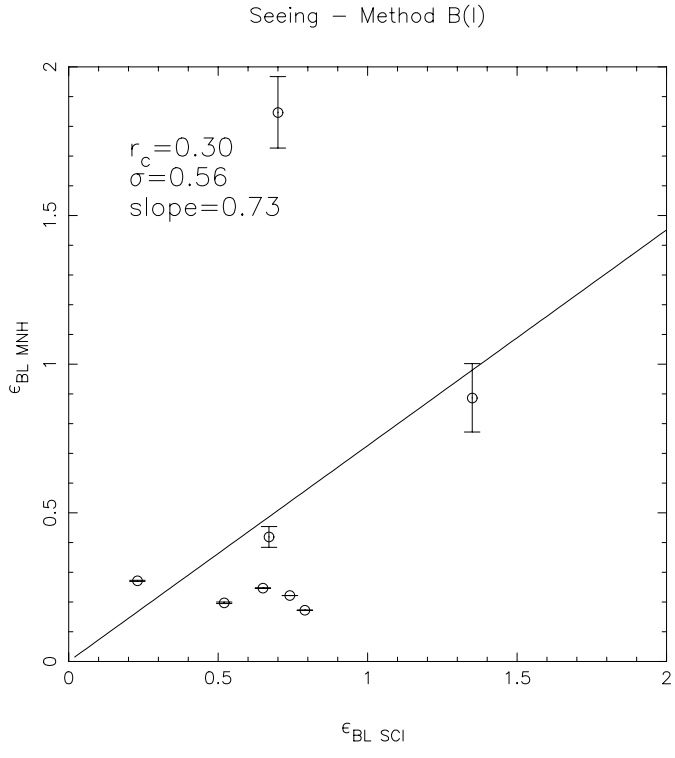


**Fig. 12.** Method B(I): statistical analysis summary for the boundary layer seeing $\varepsilon_{\rm BL}$. The calibration coefficient is $\beta = 4.48$ (Table 3)

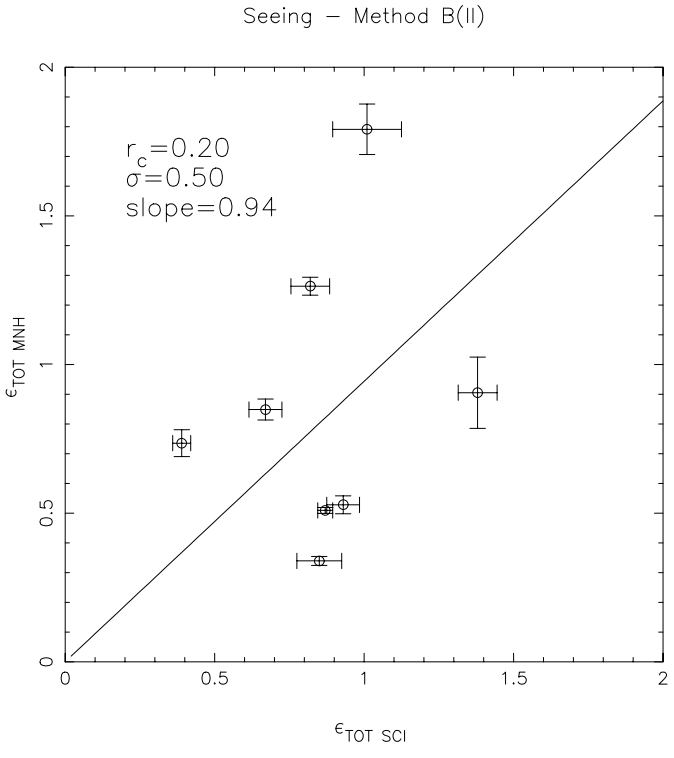


**Fig. 14.** Method B(II): statistical analysis summary for the total seeing $\varepsilon_{\rm Tot}$. The calibration coefficient is $\beta = 2.86$ (Table 3)

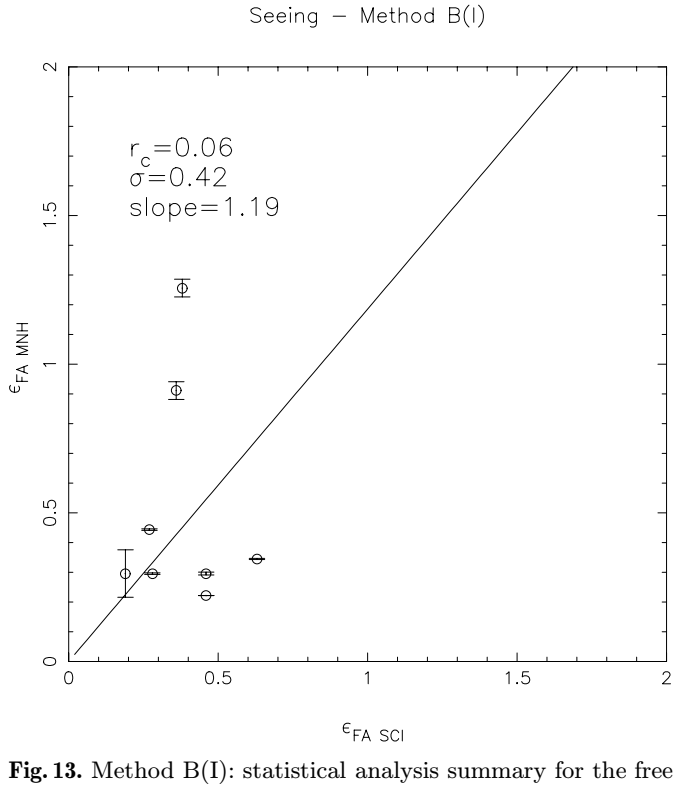


**Fig. 13.** Method B(I): statistical analysis summary for the free atmosphere seeing $\varepsilon_{\rm FA}$. The calibration coefficient is $\beta = 4.48$ (Table 3)

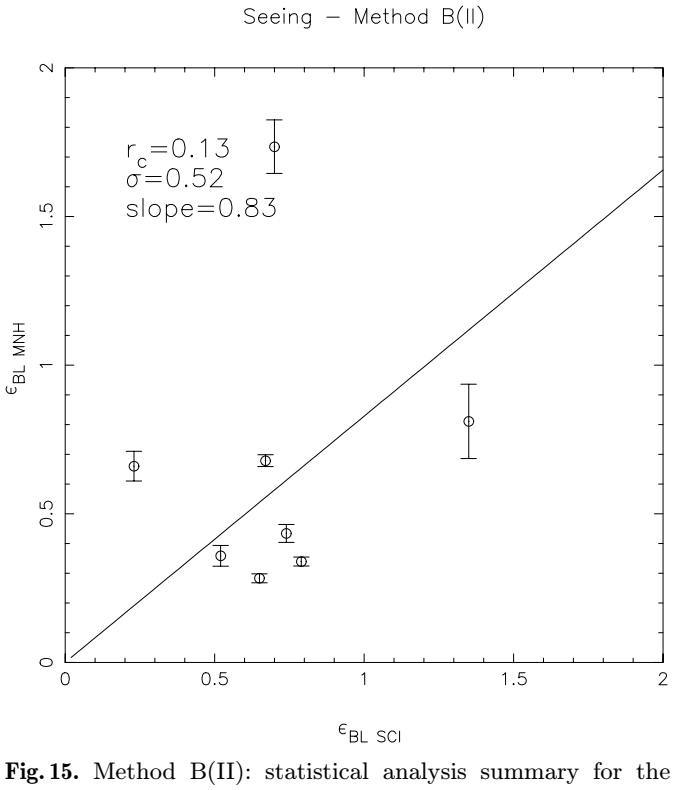


**Fig. 15.** Method B(II): statistical analysis summary for the boundary layer seeing $\varepsilon_{\rm BL}$. The calibration coefficient is $\beta = 2.86$ (Table 3)

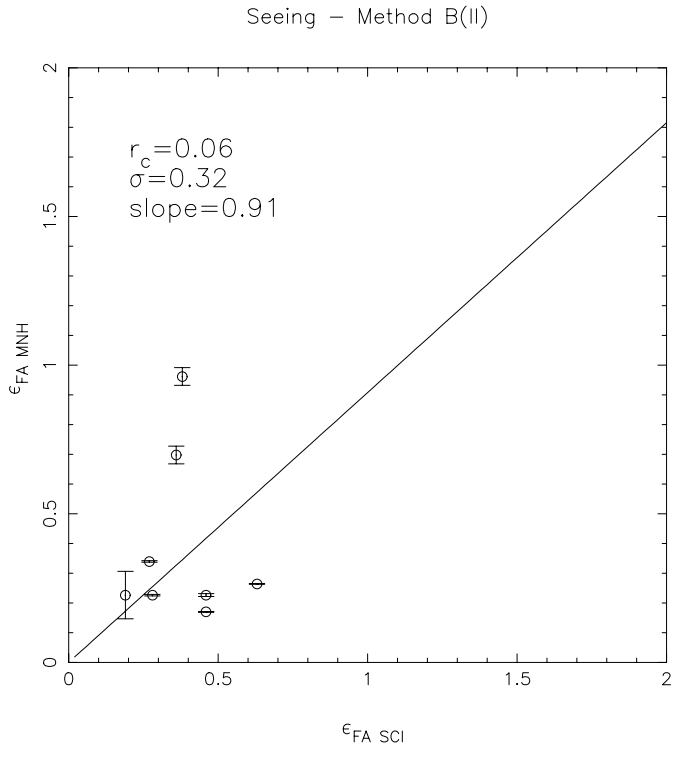


**Fig. 16.** Method B(II): statistical analysis summary for the free atmosphere seeing $\varepsilon_{\rm FA}$. The calibration coefficient is $\beta = 2.86$ (Table 3)

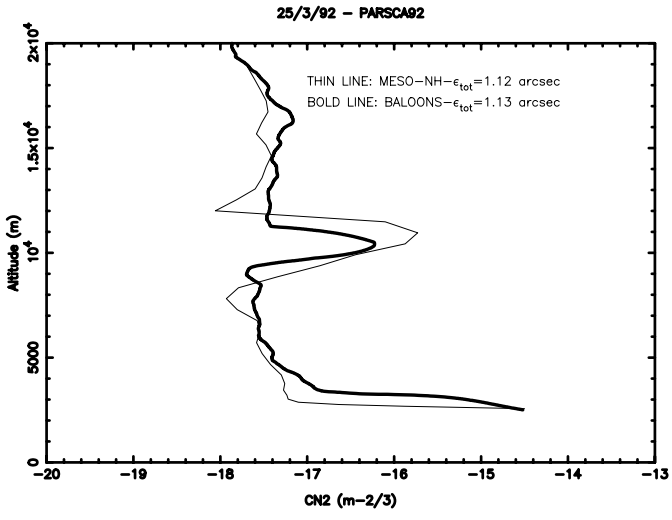


**Fig. 17.** $C_{\rm N}^2$ profiles comparison from balloons (full line) and Meso-Nh simulations after a 3 - hour simulation (thin line) on 25 Mars 1992. Calibration coefficient $\beta = 1.66$

to the $C_{\rm N}^2$ profiles, can analyze model performances on selected parts of the atmosphere. In particular, as we will see later,we can study separately the boundary layer and the free atmosphere.

We discussed, until now, the results from a global point of view. Can we have a finer analysis of the estimation of the energy in the low and in the high part of the atmosphere? Using both Methods A and B, we achieve correlation coefficients smaller than that characterizing the optical measurements (see $r_{\rm c} = 0.82$ in Sect. 2). Looking at the Figs. 12, 13 and Figs. 15, 16 it is obvious that the correlation level, especially in the high part of the atmosphere ($\varepsilon_{\rm FA}$) is weak. Analyzing the whole campaign, night by night, we remarked that this fact is due to a poor reliability of the Antofagasta radiosounding that often provides erroneous vertical ($p$, $T$ and $\boldsymbol{V}$) profiles in the middle atmosphere. In this case, the model generates unrealistic $C_{\rm N}^2$ layers which hamper the statistical analysis (Masciadri et al. 1997). We found that, frequently, the dynamic instability generated by the model is related to the radiosounding temperature profiles.

In the analyzed cases (with and without the first 106 m of atmosphere) the slopes of the regression line (after calibration) related to $\varepsilon_{\rm BL}$ and $\varepsilon_{\rm FA}$ are of the same order of magnitude. This means that the model has a comparable sensitivity in both the low and high parts of the atmosphere.

In the boundary layer, in both the Methods B(I) and B(II) there is a small systematic tendency of the model to underestimate the turbulence. In fact the slope is, in both cases, smaller than 1. It is possible that a better configuration of the model near the ground could give better results. In particular, as explained in the next section, the ground radiative contribution in the global energy budget, could be an important element. In the free atmosphere, the correlation coefficient is not good but the points are distributed in a more random way than in the boundary layer. We suppose that, in this case, no systematic error is made by the model.

In any case, we can show that in particular favorable conditions, the model can simulate a good optical turbulence distribution in the free atmosphere as shown in Fig. 17. The measured $C_{\rm N}^2$ profile is obtained by a balloon launched during the PARSCA92 campaign. A favorable condition means that a deep region in the troposphere has a weak stability associated to a strong gradient of the wind. A good $C_{\rm N}^2$ profile reconstruction at these high altitudes is very interesting for the scintillation rate, the isoplanatic angle and the wavefront coherence time forecasts. All these parameters are very sensitive to this kind of turbulence. In particular, the predictive performance of the wavefront coherence time could be extremely good. We know, that its sensitivity increases with the 5/3 power of wind intensity. At these latitudes the jet stream wind speed can reach 60 m/s and it becomes an important parameter. Knowing that the wind prediction at the synoptic scales is generally reliable, this numerical technique could give good forecasts of the wavefront coherence time.

In order to estimate the statistical reliability of our technique, we compared the statistical estimators presented in the previous paragraph with those obtained by a simple forecast-by-persistence method.

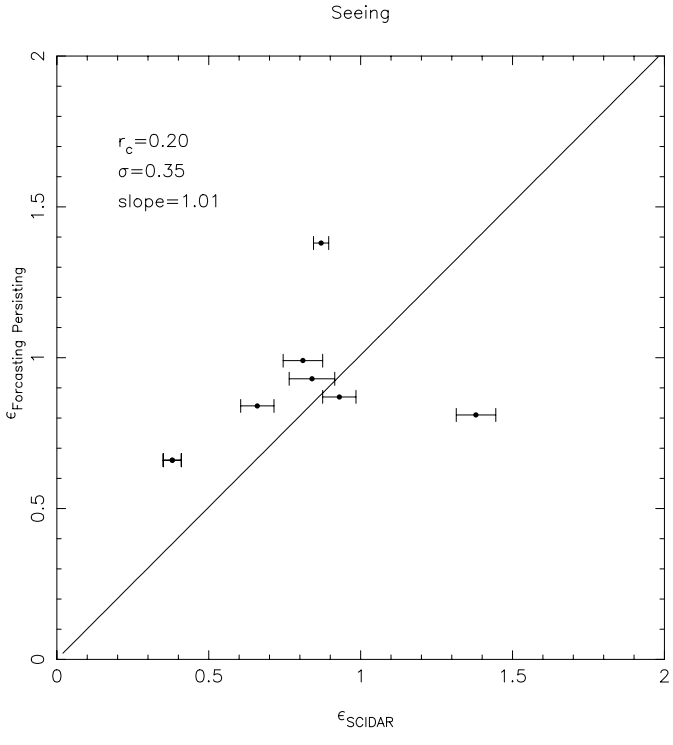


**Fig. 18.** Statistical analysis comparison between the forecast by persistence and Scidar measurements

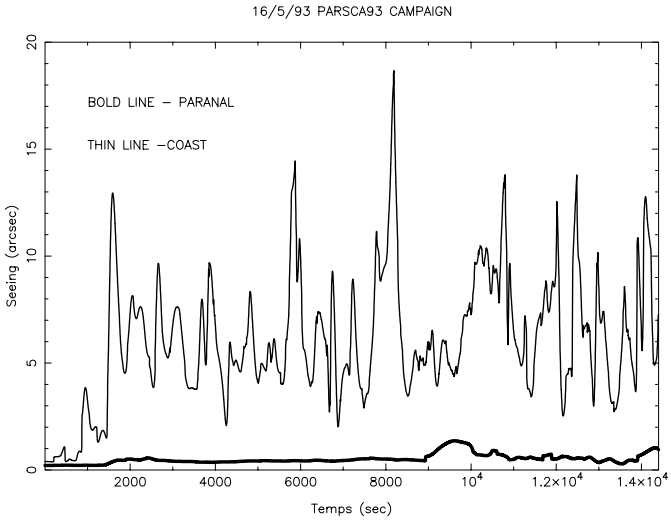


**Fig. 19.** Temporal evolution of the seeing over a 4 hour simulation time above the Paranal mountain and the chilean cost on 16 May 1993 night

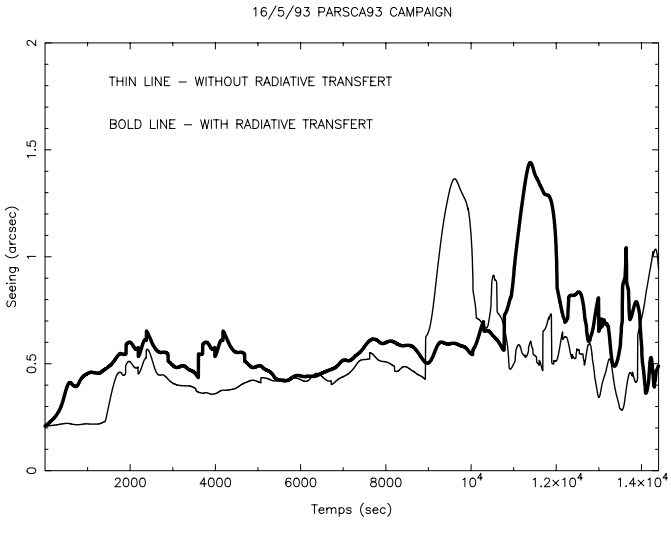


**Fig. 20.** Temporal evolution of the seeing over a 4 hour simulation time, with a radiative scheme (full line) and without it (thin line) during the 16 May 1993

The forecast-by-persistence principle is based on the assumption that the seeing of the next night is the same as that of the present night. It gives good results especially during periods characterized by a stable weather. It fails when an abrupt modification of the atmospheric state occurs. In other words, the numerical technique could be useful when the persistence method fails. We constructed a sequence of seeing values following the principle just described: the seeing of the $(J+1)$-th night is equal to the seeing of the $J$-th night. We computed all the statistical estimators between Scidar measurements and this sequence of values. Figure 18 shows the results of this analysis.

This result is compared to those obtained using Methods A and B. Following the criterion of the maximum correlation coefficient, the numerical Methods A, B(I) and B(II) give better results: $r_{\mathrm{c,MNH}} > r_{\mathrm{c,persistence}}$. Conversely, following the criterion of the minimum standard deviation, the forecast-by-persistence method gives better results: $\sigma_{\mathrm{persistence}} < \sigma_{\mathrm{MNH}}$. No conclusions can be drawn because of the small number of statistical points.

We recall that during PARSCA93 the weather was particularly favorable to the forecasting-by-persistence because we identified two periods characterized by a worse ($\overline{\varepsilon} = 0.94$ for the 13-19 May nights) and a better ($\overline{\varepsilon} = 0.57$ for the 20-26 May nights) seeing with respect to a mean value over the whole campaign $\overline{\varepsilon} = 0.75$. During each period, the statistical fluctuations around these mean values are not great. Under these conditions the forecast by persistence method is particularly efficient. Hence, we can expect that under a realistic conditions (for example a longer campaign or over many campaigns in different part of the year), the forecast by persistence method might give worse results.

The present study confirms the good geographic location of the Paranal site. Most of the simulations (Figs. 35-42 in Masciadri et al. 1997) show that Paranal mountain is sufficiently far from the Chilean coast which is characterized, on the contrary, by a high turbulence production rate. To give an example of the different turbulence production over the coast and the Paranal mountain, we report, in Fig. 19, the temporal seeing

evolution over a 4 hours simulation related to the 16 May night.

Finally, important elements concerning the sensitivity and precision of the model appeared at the end of this study. We considered the worst ($\varepsilon = 1.38$) and the best ($\varepsilon = 0.38$) seeing night of the PARSCA93 campaign (Table 1). We compared the seeing simulated by Meso-Nh after 4 hours simulation time and the seeing measured by Scidar during these two nights over the whole atmosphere. The ratio between the worst and the best seeing is $\varepsilon_{16}/\varepsilon_{25} = 3.6$ for the Scidar and $\varepsilon_{16}/\varepsilon_{25} = 3.8$ for Meso-Nh. This means that the model is capable of discriminating seeing values in a range [0.38 − 1.38 arcsec] typical for good sites. In the previously study (Bougeault et al. 1995) the model has shown important limitations for simulations of good seeing nights. Low seeing values were analyzed but the best spatial correlation between measurements and simulations was found at 9 km from the peak.

The ability to simulate the favorable geographic position of Paranal mountain and to discriminate between such low seeing values are positive elements for a future implementation of such a model for flexible scheduling of telescope usage.

## 6. Radiative transfer contribution

It is known that the boundary layer (BL) has a different evolution during the daytime and the nighttime (André 1978). We can distinguish two phases: during the day we see, especially in clear atmosphere conditions, the development of a convective layer whose thickness is of the order of 1 km, during nighttime, a strong thermal inversion process can decrease this layer to 30 m.

In order to describe the convective process we need a sophisticated treatment of the turbulence (Wyngaard et al. 1971). To describe the thermal nightly inversion the principal difficulty is represented by the turbulence-radiative transfer interaction and the description of turbulence in a strongly stable thermal stratification (Mahart 1985).

It is known that many difficulties are encountered if one tries to use the same model to simulate daily and nightly conditions (Wyngaard & Coté 1971). The radiative contribution in the analysis of the boundary layer has been tested and confirmed by many authors. It has not yet been proved, on the contrary, that the radiative transfer is relevant for our simulations that take care of the whole atmosphere. Besides that, the Meso-Nh model has been conceived to simulate daytime and nighttime conditions as well but using a radiative scheme one needs a description of the ground characteristic: air temperature above the ground, ground temperature, humidity and roughness. Having no detailed measurements of ground parameters, following climatological assumptions, we tested the model with a temperature difference $\Delta T = 1$ degree between the ground and the upper air. Figure 20 shows the seeing evolution over 4 hours simulation time during the 16 May night obtained with and without radiative transfer. We can conclude that the simulation with radiative scheme resolves more turbulence and this contribution seems not negligible.

We thus recommend, in the future, a systematic study using this configuration.

## 7. Conclusion and perspectives

We demonstrated that our simulations give realistic results. A non-hydrostatic model, well adapted to put in evidence the orographic effects on the development of the gravity waves, reproduces a seeing characterized by an extended turbulent region over the Chilean coast and by general low turbulence levels over the Paranal mountain site. This numerical technique could be thus efficiently used for site testing studies.

Analyzing the whole PARSCA93 campaign we conclude that the adaptation time to the orography is never smaller than 30 min. In most of the cases the model fluctuates around a stationary mean value and it does not diverge. Moreover, the time window $[2^{\mathrm{h}} - 3^{\mathrm{h}}]$ seems to give the best results following two different criteria: the correlation between the Scidar measurements and the Meso-Nh simulations is maximum and the standard deviation to the regression straight line is minimum.

We demonstrated that the model has a good sensitivity and can discriminate the worst from the best seeing of the campaign i.e. from 0.38 to 1.38 arcsec.

The turbulence rate simulated by the model is well estimated both in the low and high part of the atmosphere. We remember briefly the turbulent layer developed in 16 May night after 4 hours simulations time (Fig. 8 in Masciadri et al. 1998) and the layer resolved by the model at 10 km in 25 Mars 1992 nigh (Fig. 17).

For the first time we show that is necessary to retrieve $C_{\mathrm{N}}^2$ profiles and thence the seeing. Using only integrated values without knowledge of the vertical turbulence distribution, one could expect a wrong estimation of the simulation time.

This study can provide complementary information for the feasibility of the seeing forecasting with ECMWF products (Benzi et al. 1996). In this paper it was proved that the ECMWF products give a good ground temperature prediction. We have shown that, to use a numerical technique, it is not sufficient to forecast the ground temperature well. It is necessary to assure the quality of the observed data in the whole atmosphere.

We proved that the poor quality of the Antofagasta radiosoundings is the main cause of unstable simulations obtained during a few nights. In these cases, unrealistic dynamic instabilities are produced by the model in the

middle and high part of the atmosphere. The Antofagasta radiosoundings have a sufficient vertical resolution but are not completely reliable, at least in the limited temporal period analyzed (only 8 nights). We compared our numerical technique with the forecasting-by-persistence one but no conclusive statements can be provided for the following reasons:

- The sample analyzed is statistically poor.
- A comparison with the forecast by persistence method might be significant only on a longer period.

Antofagasta radiosoundings seem not to be of extremely good quality but it is true that:

- The Antofagasta radiosoundings are not the only products supplied by the Meteorologic Centers and others kinds of data could be analyzed. We know that analysis sampled on 31 pressure levels instead of 15 levels are provided by the ECMWF.
- During this study radiosoundings and ECMWF analysis of May 1993 have been used. Today the operational meteorological centers dispose of more and more heterogenous data in type and quality and they are not necessarily provided at synoptic hours (00:00 U.T., 06:00 U.T., 12:00 U.T. and 18:00 U.T.). The developement of new observational systems such as geostationary satellites provides a lot of informations with a high spatial and temporal resolution that can add to the data in the regions in which the observation density is poor. New methods of data assimilation are necessary to treat this new kind of data. In the last years consistent progress was made in developing new and more powerful assimilation schemes (3D and 4D variational schemes) that can integrate all the heterogeneous measurements which we have at our disposal today (Bouttier & Rabier 1998). We know that the ECMWF forecasting quality has become better and better in these last years. It could be interesting to test the model performance on more recent measurements to estimate if this progress in the forecasting science is valuable for our simulations.

## ANNEX 1: Data assimilation and data quality

The aim of the analysis (User Guide to ECMWF Products, 1995) is to provide the general circulation numerical model with the most realistic state of the atmosphere. For so doing the ECMWF uses a finite number of observations and a **first guess** provided by the same forecasting model (generally the last six hours prevision) or by climatology. The analysis must modify this first guess integrating in the best way the information coming from the observations which, in general, do not describe perfectly the atmospheric state. Different quality controls are performed on the observations in order to select a realistic set of data. The assimilation of the first guess and the observations are made using an algorithm named **optimal interpolation**. If A is the analyzed parameter, for each grid point one defines:

$$a_k^{\rm a} = a_k^{\rm g} + \sum_i \lambda_i \, (y_i^{\rm o} - y_i^{\rm g}) \tag{7}$$

where

- $a_k^{\rm a}$ is the value of A that we want to know in the $k$ grid point;
- $a_k^{\rm g}$ is the value of the parameter provided by the first guess in the $k$ grid point;
- $\lambda_i$ is the averaged weight associated to the quality of the observation (kind of measurement and kind of observed parameter), the distance between the analysis grid point and the observations grid point and the quality of the first guess;
- $y_i^{\rm o}$ is the observed value of the parameter $Y$ ($Y$ can be A or, more generally, a parameter linearly correlated to A);
- $y_i^{\rm g}$ is the value of $Y$ provided by the first guess.

The optimal interpolation method defines $\lambda_i$ in the following way:

$$\lambda_i = \frac{\sigma_{\rm g}^2}{\sigma_{o,i}^2 + \sigma_{\rm g}^2} \tag{8}$$

which transforms the Eq. (7) into

$$a_k^{\rm a} = a_k^{\rm g} + \sum_i \frac{\sigma_{\rm g}^2}{\sigma_{o,i}^2 + \sigma_{\rm g}^2} \, (y_i^{\rm o} - y_i^{\rm g}) \tag{9}$$

where $\sigma_{o,i}^2$ is the variance of observational errors, $\sigma_{\rm g}^2$ is the variance of the first guess error resulting from the total uncertainty in the analysis. When an observation is unreliable, $\sigma_{o,i}^2$ is large and $a_k^{\rm a}$ takes the value of $a_k^{\rm g}$. In this case there is a little impact on the first guess. When the observation is assumed to be accurate, $\sigma_{o,i}^2$ is small and $a_k^{\rm a}$ almost takes the value $y_i^{\rm o}$.

This analysis, named **uninitialized analysis**, can sometimes generate, fictitious gravity waves during the simulations. To avoid this, they must be initialized in order to be adapted to the dynamics of the model. This more elaborate analysis is named **initialized analysis**.

In an operational schedule, the ECMWF produces global analysis and predictions using data collected during time. The predictions are permanently corrected by the observations that are injected in the algorithm of the optimal interpolation. This feed-back system of assimilation data is named **Analysis Assimilation.**

*Acknowledgements.* This work is supported by contract (Technical Report UNI-17400-0004) from ESO. The authors are grateful to M.Sarazin for his constant and dedicated presence in this feasibility study. They wish to thank the GMME team of the Centre National de Recherche Meteorologique for their scientific collaboration and logistical help. In particular, they gratefully acknowledge the many helpful discussions with J. Stein, P. Jabouille, J.L. Redelsperger and J.P. Lafore. The authors thank C. Coulman for his helpful comments and revision of the draft.

## References

André J.C., et al., 1978, J. Atmosph. Sci. 35, 1861
Benzi, et al., 1996, Feasibility study of meteorological prediction model for ESO observatories in Chile, Report 45060/VLT/95/6952/GWI
Bougeault P., et al., 1995, Appl. Opt. 34, 3481
Bouttier F., Rabier F., 1998, ECMWF Newslett. 78, 2-5 (Winter 97/98)
Chester S., Gardner et al., 1990, Proceedings of the IEEE 78, 1721
Fuchs A., Vernin J., 1994, VLT technical Report VLT-TREUNI-17400-0001
Mahart L., 1985, J. Atmosph. Sci. 42, 2333
Masciadri E., et al., 1997, Feasibility study of seeing prevision using the Meso-Nh meteorological model, ESO- Report 47724/VLT/96/6384/MST, December 1997
Masciadri E., et al., 1998, A&A (submitted) (Paper I)
Morand F., Piriou C., 1995, Guide à l'usage des utilisateurs du model Arpège (22 December 1995)
Press W.H., et al., 1989, Numerical Recipies Fortran Version
User Guide to ECMWF Products Meteorologic Bulletin M 3.2 (22 December 1995)
Wyngaard J.C., et al., 1971, J. Opt. Soc. Am. 61, 1646
Wyngaard J.C., Coté O.R., 1971, J. Atmosph. Sci. 28, 190